CrystEngComm

Accepted Manuscript

ROYAL SOCIETY OF CHEMISTRY

www.rsc.org/crystengcomm

Journal Name

RSCPublishing

ARTICLE

Controllable Morphology and Tunable Colors of Mg and Eu ions co-doped ZnO by Thermal Annealing

Cite this: DOI: 10.1039/x0xx00000x

S. Yang [a, b, c], D. L. Han [a, b, c], M. Gao[c], J. H. Yang [c*] and Bayanheshig [a]

Received 00th January 2012,
Accepted 00th January 2012

DOI: 10.1039/x0xx00000x

www.rsc.org/

Mg^{2+} and Eu^{3+} co-doping ZnO nanostructure were prepared by an environmentally friendly method. With an increasing annealing temperature, the Mg^{2+} and Eu^{3+} co-doping ZnO nanosheet crystallites in aggregates experienced the structural evolution from individual nanochain to partially sintered short rods and finally smooth nanorods. Consequently, the optical properties in Mg^{2+} and Eu^{3+} co-doping ZnO were changed accordingly, as shown here for white, green and yellow emitting segments. This study on the correlation between sintered structure and optical properties shows that controlled thermal annealing affecting stress through the structural evolution of the Mg^{2+} and Eu^{3+} co-doping ZnO nanocrystallites.

Introduction

Chemically stable and highly emissive phosphor materials are always in demand for display and lighting applications. The majority of the commercially available phosphors are expensive, so it is necessary to develop innovative materials with improved luminous efficacy, energy-saving and low-power consumption characteristics. Among the commercially available phosphors, [1, 2] ZnO is considered as a promising material for optoelectronic devices, [3-6] such as light-emitting diodes (LEDs), due to its large and direct band gap (3.36 eV), and high exciton binding energy (60 meV) at room temperature. [7] For pure ZnO, usually, its native optical properties are not good enough for the high requirement in the practice applications. Fortunately, the embedded dopants in a single crystalline nanostructure would enable some novel physical properties come out, such as ferromagnetism, bandgap renormalization, high conductivity, electron-phonon coupling effect, and catalytic activity modification. [8, 9]

Doping wide bandgap materials with trivalent rare earth (RE) ions is well known to enhance the optical activity. The intra-4f emission spectra of rare earth ions are characterized by narrow lines with high color purity because the 4f electrons of rare earth ions are shielded by the outer 5s and 5p electrons from external forces. In addition, the positions of the 4f configuration energy levels are only slightly dependent on the host matrix, and are roughly the same as the free-ion levels. [10] These unique properties are of interest in development of new materials with the capability to produce visible light with narrow lines for red, green, and blue phosphors. Among other rare earths, Eu^{3+} has received great interest because of its strong red $^5D_0$ $^{-7}F_2$ emissions. [10, 11] But it is difficult for Eu^{3+} to enter ZnO host lattice due to the large ionic radius mismatching between the ionic radii of Zn^{2+} (0.75 Å) and Eu^{3+} (0.95 Å) and it could hamper the energy transfer from the host to the Eu^{3+} ions. [12] In the previous works, we have studied the Eu^{3+}, Mg^{2+} codoped ZnO for enhance the Eu^{3+} emission intensity. The results showed that the intensity of the Eu^{3+} emission is related to the defects of oxygen vacancies and surface defects caused by Mg doping. It is well known that the crystal quality of material not only depends on growth methods but also on the postheating treatments such as annealing. Annealing temperature is considered as crucial factors for crystalline quality, oxygen defects, and optical property of semiconductor oxides. So it remains an open question regarding how to optimize the red emission through defect engineering.

In this study, annealing effect is investigated in order to understand the structural and optical property evolution of Mg^{2+} and Eu^{3+} co-doping ZnO nanostructure (ZMEO). Finally, we get three different emitting segments through controlling temperature, which will prompt the future applications of rare earth doped ZnO nanomaterials in advanced display and lighting application.

Experimental

ZMEO Preparation

ZMEO nanostructures are synthesized using a two-step method comprising hydrothermal precursor preparation and annealing. All starting reagents used in this experiment were analytical grade. Eu_2O_3 (99.9%) was dissolved in HNO_3 to obtain 0.01 M $Eu(NO_3)_3$ solutions. $Zn(NO_3)_2{\cdot}6H_2O$ was dissolved in deionized water, then appropriate amount of $Mg(NO_3)_2$, and $Eu(NO_3)_3$ were added to the solution to a molar ratio of 0.9: 0.09: 0.01 for Zn/Mg/Eu. The solution of NH_4HCO_3 was added into the former mixture solution, and the white precipitations formed immediately. The mixture was stirring for 4h. After this procedure, a clear -Zn-O-Eu- and -Zn-O-Mg- precursor solution was obtained. The finally obtained precipitates were isolated by centrifugation, cleaned in acetone and ethanol following standard cleaning procedures in a cleanroom environment, and kept in the drying cabinet at 80 °C for one day. We named as-grown sample ZMEO. For better

crystallinity and enhanced luminescence, the sample was further annealed in air for 1 h at 300, 400, 500, 600 and 700 °C, respectively.

Characterization

We evaluated the structural quality of samples with X-ray diffraction (XRD, MAC Science, MXP18, Japan). The incident side of the x-rays employed a double-crystal Ge (220) monochromator with Cu Kα radiation at 1.5406 Å. The detector side employed a Ge (220) analyzer to achieving a high 2Θ resolution of 0.02º. The morphology of the samples was characterized by JEOL JSM-6700F field emission scanning electron microscope (FE-SEM). Room temperature photoluminescence (PL) measurement was measured using Renishaw inVia Raman system under a 325 nm (or 3.815 eV) He-Cd laser (30 mW) and a 514.5 nm (or 2.41 eV) Ar^+ ion laser (20 mW) excitation. Here the PL emissions, dispersed in a 0.5 m single monochromator equipped with a grating of 2400 grooves cm^{-1}, were detected with CCD. The 514.5 nm radiation from a 20 mW water-cooled argon ion laser was used as the exciting source. A 50 × and 15 × Leica object with a long working distance focused the excitation beam onto the samples with a spot size of ca 1~2 μm.

Results and discussion

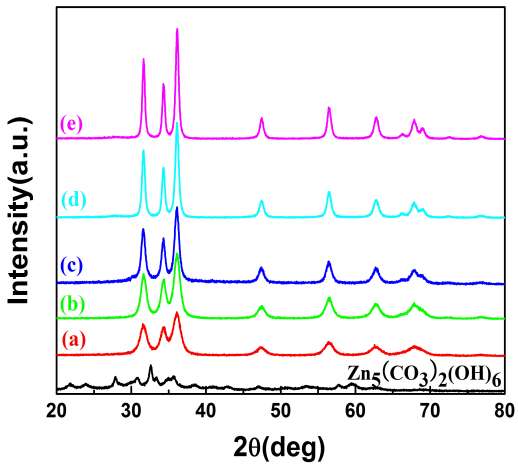

Fig. 1 XRD pattern of as-synthesized ZMEO samples at different annealing temperature (a) 300 °C, (b) 400 °C, (c) 500 °C, (d) 600 °C, and (e) 700 °C; Below figure (a) shows the initial of the ZMEO before annealing.

Thermal annealing-temperature-dependent XRD spectra of ZMEO samples are presented in Figs. 1. All the diffraction peaks are well indexed according to the hexagonal phase ZnO as reported in JCPDS card (no. 36-1451). It is seen that thermal annealing did not create any extrinsic phase but improved the crystal quality of ZMEO, as manifested by the XRD pattern remaining unchanged except for a reduction in linewidth. These data also reveal that the most preferred orientation is along the (101) reflection plane for all the annealed samples. While, we can see the initial product below the Fig 1 (a) is not ZnO but the hydroxide zinc carbonate ($Zn_5(CO_3)_2(OH)_6$), which is easily pyrolyzed into ZnO by further annealing. In addition, it was noteworthy that no secondary phases including Mg and Eu alloys were detected in the XRD measurements, and this confirmed proper incorporation of dopant atoms inside ZnO crystal lattice.

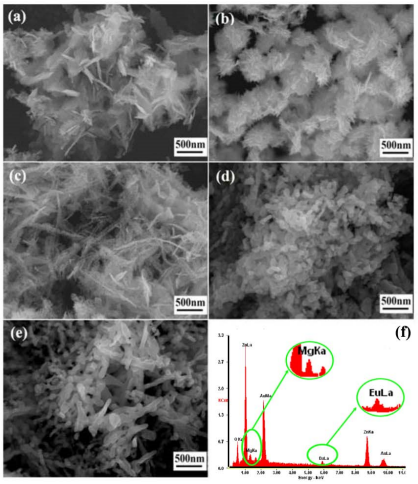

Fig. 2 Typical FESEM image of (a) ZMEO annealed at 300 °C; (b) ZMEO annealed at 400 °C; (c) ZMEO annealed at 500 °C; (d) ZMEO annealed at 600 °C; (e) ZMEO annealed at 700 °C; (f) EDS of as-synthesized ZMEO samples annealed at 700°C.

The annealing temperature had a dominative influence on the microscopic structure and the morphology of ZMEO. As the temperature rose, the ZMEO showed different morphologies. The SEM micrographs of the ZMEO powder after annealing at 300~700 °C are shown in Fig. 2(a) ~ (e). Figure 2a shows that the sample was flower-like structure after annealing at 300°C. A full flower-like hierarchical structure formed when the annealing temperature was 400°C, and the size was about 2 μm (Figure 2b). Fig. 2c shows the SEM images of the ZEMO annealing at 500°C. The samples are nanochains comprised by nanoparticals. The lengths of nanochains in Fig. 2c are about 1 μm. However, the samples are transformed into short nanorods after annealing at 600°C, the length of the rods is 300 nm as shown in Fig. 2d. In Fig. 2e, the sample consisted of a large amount of straight and smooth nanorods with 150-300 nm diameter and 1-2 μm length and less nanoparticles. It is noteworthy that the nanorods in annealed 700°C are larger than in 600°C. The compositions were also studied by EDS equipped in SEM as shown in Fig. 2f. Eu and Mg peaks are evident in the spectrum. Similar amounts of Eu concentration are observed at different detecting points of ZMEO, and the nominal Mg and Eu content in the products is estimated to be 4.5% and 1.03%, respectively.

Further morphological characterization of the ZMEO samples was carried out by TEM. A TEM image of the ZMEO micrograph that the nanosheet in shape with irregular small annealed at 300°C is presented in Fig. 3a. It is clear from the porous microstructure. The size of the porous is about 10 nm. The reasons of form this morphology can be explained as follows: The synthesis consists of two steps: hydrothermal and annealed process. We chose the hydrothermal method to get efficient doping of Eu and Mg ions, because the anion-rich environment associated with the chemical route greatly benefits the doping process by suppressing the "self-purification" mechanism, leading to homogeneous ions doping. [15] The decomposition of ammonium bicarbonate produced OH^- and CO_3^{2-} anions, which would form precipitates with Zn^{2+} cations, such as $Zn_5(CO_3)_2(OH)_6$. OH^- ions were formed as a result of the reaction of HCO_3^- with H_2O, and CO_3^{2-} was produced by the reaction of CO_2 with OH^-. The reaction can be expressed as follows:

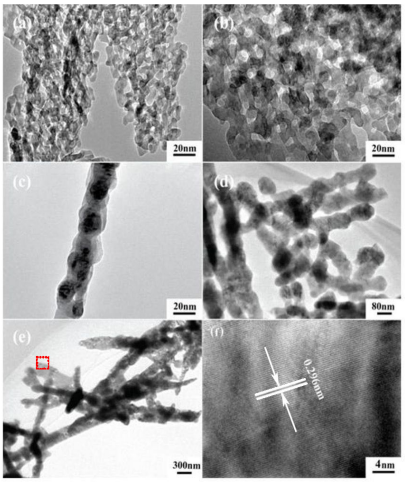

Fig. 3 Typical TEM image of (a) ZMEO annealed at 300 °C; (b) ZMEO annealed at 400 °C; (c) ZMEO annealed at 500 °C; (d) ZMEO annealed at 600 °C; (e) ZMEO annealed at 700 °C; (f) HRTEM of as-synthesized ZMEO samples annealed at 700°C.

$$NH_4HCO_3 \rightarrow NH_4^+ + HCO_3^- \quad (1)$$
$$HCO_3^- + H_2O \leftrightarrow OH^- + H_2O + CO_2 \quad (2)$$
$$2OH^- + CO_2 \leftrightarrow CO_3^{2-} + H_2O \quad (3)$$
$$2CO_3^{2-} + 6OH^- + 5Zn^{2+} \leftrightarrow Zn_5(CO_3)_2(OH)_6(s) \quad (4)$$

In the annealed process, the precursors can be decomposed into wurtzite ZnO after further annealing. Due to the loss of volatile gas such as H_2O and CO_2 released during the annealed process, the ZnO nanosheets with mesoporous structure are formed, which can be expressed by the Eq. (5).

$$Zn_5(CO_3)_2(OH)_6 \rightarrow 5ZnO + CO_2 + 3H_2O \quad (5)$$

During above chemical process, the Mg and Eu ions have doped into ZnO and formed nanosheets with mesoporous structure. By comparing Fig. 3a and 3b, it is evident that the porous size for the ZMEO sample annealed at 300°C is much smaller (~10 nm) than that for the sample annealed at 400°C (~20 nm). The corresponding TEM images show that the diameter of the nanochains is 40 nm at 500°C. The samples are transformed into short nanorods when the temperature increased 600°C as shown in Fig. 3d. The length of short nanorod is ~300 nm and the diameter is about 80 nm. In Fig. 3e, the nanorods became longer and thicker. The length of the nanorod is 1~2 µm and the diameter is about 300 nm. This can be partly explained by the aggregation of nanorods. The nanorods are in the form of clusters caused by aggregation, as indicated in the TEM. During the high-temperature annealing, the clusters will melt and recrystallize into larger nanorods. [16] The higher Gibbs free energy of smaller nanorods may also contribute to the process. Thus, the nanorods annealing at 700°C are less thermodynamically stable, fusing into larger nanorods. The HRTEM image in Fig. 3f was taken out at the top area marked by red dot box in Fig. 3e. It clearly reveals the nanorod grow along the [0 0 0 1] direction, and no secondary phase or impurity was observed. [17] The distance between two adjacent planes estimated from the lattice fringes is found to be 0.296 nm, which is bigger than ZnO (0.266 nm). [18] Hence, the increase in lattice spacing is a good indicator of successful doping of Eu^{3+} ions in ZnO lattice.

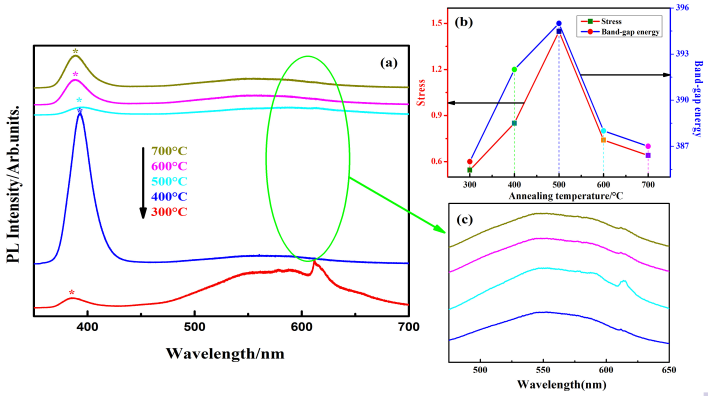

Fig. 4 (a) room temperature PL spectra of ZMEO at different annealing temperature under the direct excitation of 325 nm wavelength; (b) the band-gap energy and the tensile stress of the ZMEO as a function of temperature; (c) the enlarge part of the PL spectra between 450 and 650 nm.

The room temperature photoluminescence study on the annealed samples has been carried out to investigate optical properties of ZMEO. Figure 4 depicts the comparison of ZMEO at different annealing temperature. All of them are consists of a UV peak, a DLE band in the range of 430~650 nm and an additional sharp red emission peak centering at 613 nm (as shown in Fig. 4a). The UV emission band is related to a near band-edge transition of ZnO, namely, the recombination of the free excitons and the visible emission band produced by transition of excited optical center from deep level to the valance level. This kind of deep level emission is due to presence of oxygen vacancies or zinc interstitials. [19-21] As seen in the figure, with increasing the annealing temperatures, the UV emission redshifts to 386 nm, 392 nm, 395 nm, and blueshifts to 388 nm, respectively. With the increase of annealing temperature, the shift of band-gap energy was believed to originate from the change of tensile stress due to the lattice distortion. If the tensile was released, the band-gap energy was decreased. [22] In Fig. 4b, we compare the band-gap energy and the tensile stress of the ZMEO as a function of temperature. It can be observed that the temperature-dependent evolution of the band-gap energy follows a similar trend as the tensile stress. Fig. 4c show the enlarge part of the PL spectra between 450 and 650 nm. A sharp red emission peak centering at 613 nm was observed in ZMEO annealing at 400 °C, 500 °C, 600 °C, and 700 °C, which attributed to the intra-4f transition of Eu^{3+} ions. Our previous report have suggested that the defect complexes, i.e. oxygen vacancies and surface defects caused by Mg doping, serve as the energy storage centers to mediate the energy transfer from the ZnO host to the Eu^{3+} ion, which will strongly enhance the Eu^{3+} emission. [23]

In order to avoid band-to-band transition (~382 nm), we also took PL spectra of ZMEO under the direct excitation of 514 nm wavelength (Fig. 5). The emission peaks at 579, 519, 595, 613, 650 and 700 nm can be assigned to the $^5D_0$ - ^7F_J transitions (J = 0-4) of Eu $^{3+}$ ion. [24] The most intense emission is associated to the $^5D_0$ - $^7F_2$ transition in the red spectral region (613 nm), which correspond to the very sharp and intense excitation and emission peaks due to the well crystalline surrounding of Eu $^{3+}$ owing to the very distorted local environment.

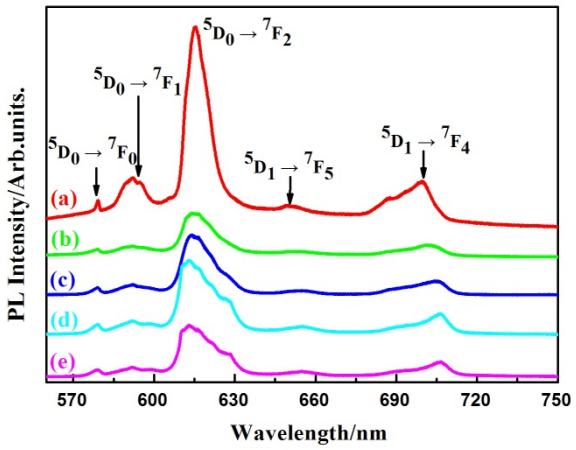

Fig. 5 room temperature PL spectra of ZMEO at different annealing temperature under the direct excitation of 514 nm wavelength

As shown in Fig. 5, the intensity of emission peaks at 613 nm, decreased at 400 °C and then increased with increasing the annealing temperature, which follows a similar trend as the intensity of DEL. The sharp and intense emissions in the range 573-630 nm of ZMEO under two excitations suggest that Eu ions may gain energy from ZnO, giving rise to an intra-4f transition. [25-27]

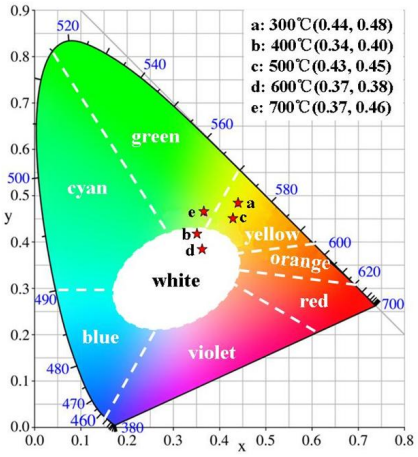

Fig. 6 CIE chromaticity diagram for ZMEO annealed at different temperature.

To understand the luminescent properties of the prepared material, CIE 1931 chromaticity coordinates are also calculated from the emission spectrum. This system offers more precision in color measurement because the parameters are based on the spectral power distribution (SPD) of the light emitted from a colored object and are factored by sensitivity curves which have been measured for the human eye. Based on the fact that the human eye has three different types of color sensitive cones, the response of the eye is best described in terms of three "tristimulus values". The colors which can be matched by combining a given set of three primary colors (such as the blue, green and red of a color television screen) are represented on the chromaticity diagram by a triangle joining the coordinates for the three colors. The corresponding diagram for chromaticity index is shown in the Fig. 6. For instance, ZMEO annealing at 700 °C were calculated to be x=0.37 and y=0.46 using equidistant wavelength method [28] and are indicated in the CIE chromaticity diagram shown in Figure 6 (for green), whereas ZMEO annealing at 400 °C and 600°C correspond with x=0.34, y=0.40 and x=0.37, y=0.38. These samples are useful for white LEDs. The chromaticity coordinates of sample a and c fall in the yellow range of visible light. The CIE chromaticity clearly shows that the ZMEO annealing at different temperatures exhibit green, yellow and white emission, respectively. The emission colors might be further finely tuned by finely changing the annealing temperatures, which is of great interest and this research is ongoing.

Conclusions

We have reported an efficient, environmentally benign, and solution approach to tune the luminescence of Mg, Eu co-doped ZnO by changing the annealing temperature. It was found that the intensities of near band edge (NBE) exitonic ultraviolet emission and the Eu^{3+} emission increased maximum at 400 °C and 300 °C respectively. Annealing temperature offers a promising way to get a sharp change of the color at the ZMEO, as shown here for white, green and yellow emitting segments. The optimal conditions generate white light with chromaticity coordinates [(0.37, 0.38) and (0.34, 0.40)]. As a result of their unique luminescence properties and controlled morphology, these samples may find potential applications in the fields of color displays, light-emitting diodes (LEDs), and solid-state lasers.

Acknowledgements

This work is supported by Program for the National Natural Science Foundation of China (Grant Nos. 11204104, 61008051, 61178074, 11254001), Program for the development of Science and Technology of Jilin province (Item No. 201215225, 201105084, 201205078 and 201215223).This work was also supported by the Vice-Chancellor's Postdoctoral Research Fellowship Program of the University of New South Wales (SIR50/PS26746).

Notes and references

[a] Changchun Institute of Optics, Fine Mechanics and Physics, Chinese Academy of Sciences, Changchun 130033, China.
[b] University of Chinese Academy of Sciences, Beijing 100049, China.
[c] Key Laboratory of Functional Materials Physics and Chemistry of the Ministry of Education, Jilin Normal University, Siping 136000, P. R. China.

1 K. Kole, C. S. Tiwary and P. Kumbhakar, *CrystEngComm,* 2013,**15**, 5515.
2 W. I. Park and G. C. Yi, *Adv. Mater.,* 2004, **16**, 87.
3 C. S. Rout and C. N. R. Rao, *Nanotechnology,* 2008, **19**, 285203.
4 S. C. Li, K. Yu, Y. Wang, Z. L. Zhang, C. Q. Song, H. H. Yin, Q. Ren and Z. Q. Zhu, *CrystEngComm,* 2013,**15**, 1753.
5 J. D. Ye, S. L. Gu, S. M. Zhu, W. Liu, S. M. Liu, R. Zhang, Y. Shi, and Y. D. Zheng, *Appl. Phys. Lett.,* 2006, **88**, 182112.

6 D. Barreca, D. Bekermann, E. Comini, A. Devi, R. A. Fischer, A. Gasparotto, C. Maccato, C. Sada, G. Sberveglieri and E. Tondello, *CrystEngComm,* 2010,**12**, 3419.
7 Z. P. Wei, Y. M. Lu, D. Z. Shen, Z. Z. Zhang, B. Yao, B. H. Li, J. Y. Zhang, D. X. Zhao, X. W. Fan, and Z. K. Tang, *Appl. Phys. Lett.,* 2007, **90**, 042113.
8 J. Xu, C. H. Liu, Z. F. Wu, *Microchimica Acta,* 2011, **172**, 425.
9 M. M. Rahman, S. B. Khan, A. M. Asiri, K. A. Alamry, A. A. P. Khan, A. Khan, M. A. Rub, *Microchimica Acta,* 2013, **180**, 675.
10 J. Jensen and A. R. Mackintosh, *Rare Earth Magnetism: Structures and Excitations (Oxford: Clarendon)*, 1991.
11 Jung-Chul Park, Hye-Kyung Moon, Dong-Kuk Kim, Song-Ho Byeon, Bong-Chul Kim, and Kyung-Soo Suh, *Appl. Phys. Lett.,* 2000, **77**, 2162.
12 A. Pillonnet, A. Berthelot, A. Pereira, O. Benamara, S. Derom, G. Colas des Francs, and A.-M. Jurdyc, *Appl. Phys. Lett.,* 2012, **100**, 153115.
13 D. D. Wang, G. Z. Xing, M. Gao, L. L. Yang, J. H. Yang, and T. Wu, *J. Phys. Chem. C,* 2011, **115**, 22729.
14 H. F. Liu and S. J. Chua, *J. Appl. Phys.*, 2009, **106**, 023511.
15 R. D. Shannon, *Acta Crystallogr. Sect. A: Cryst. Phys.*, 1976, **32**, 751.
16 M. D. Gustavo, R. C. James, *Phys. Rev. Lett*., 2006, **96**, 226802.
17 X. Su, Z. J. Zhang, and M. M. Zhu, *Appl. Phys. Lett.,* 2006, **88**, 061913.
18 G.Z. Xing, J.G. Tao, G.P. Li, Z. Zhang, L.M. Wong, S.J. Wang, C.H.A. Huan, T. Wu, *2008 2nd IEEE International Nanoelectronics Conference*, 2008, **1–3**, 462.
19 F. Ahmed, S. Kumar, N. Arshi, M. S. Anwar and B. H. Koo, *CrystEngComm*, 2012, **14**, 4016.
20 A. Wang, J. Dai, J. Cheng, M. P. chudzik, T. J. Marks, R. P. H. Chang, and C. R. Kannewurf, *Appl. Phys. Lett.,* 1998, **73**, 327 .
21 Q. H. Li, Q. Wan, Y. X. Liang, and T. H. Wang, *Appl. Phys. Lett.*, 2004, **84**, 4556.
22 H. S. Kang, J. S. Kang, J. W. Kim, and S. Y. Lee, *J. Appl. Phys.*, 2004, **95**, 1246.
23 J. Zolper, M. H. Crawford, A. J. Howard, *Appl. Phys. Lett.,* 1996, **68**, 200.
24 M. Gao, J. Yang, L. Yang, Y. Zhang, H. Liu, H. Fan, Y. Sui, B. Feng, Y. Sun, Z. Zhang and H. Song, *Science of Advanced Materials*, 2013, **5**, 346.
25 A. Bell, I. Harrison, D. Korakakis, *J. Appl. Phys.,* 2001, **89**, 1070.
26 H. Kanber, R. J. Cipolli, W. B. Henderson, *J. Appl. Phys.*, 1985, **57**, 4732.
27 H. S. Kang, J. S. Kang, S. S. Pang, *Mater. Sci. Eng. B.*, 2003, **102**, 313.
28 X. Yang, G. Du, X. Wang, *J. Cryst. Growth.*, 2003, **252**, 275.
29 J. Kelmer, *Luminescent Screens: Photometry and Colorimetry (Iliffe, Lond)*, 1969, 118.

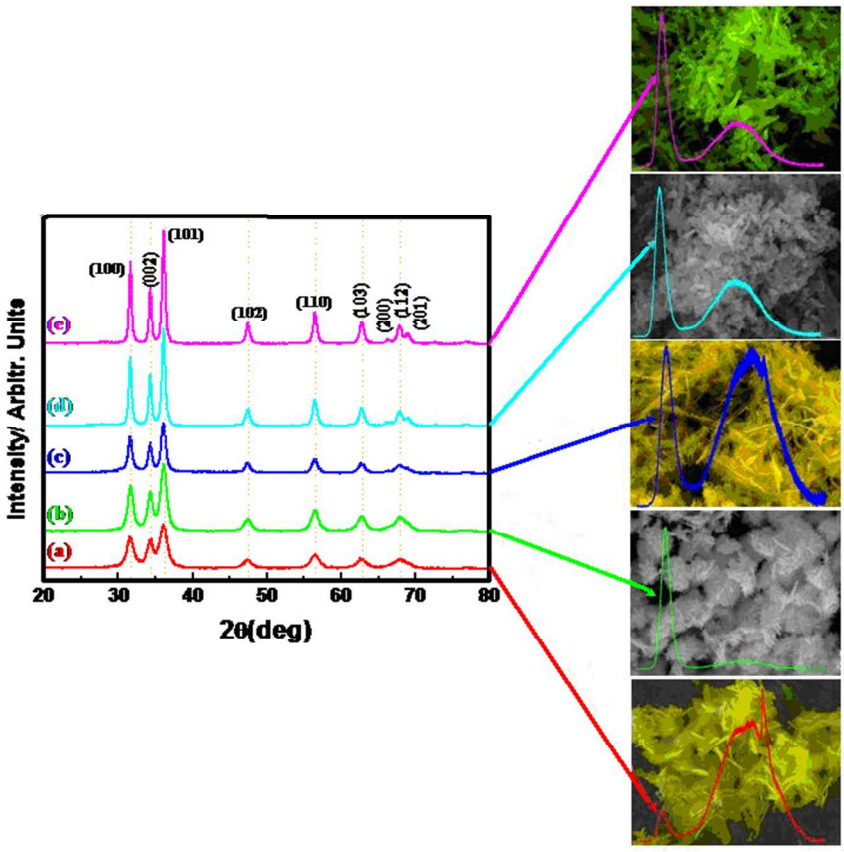

Controllable Morphology and Tunable Colors of Mg and Eu ions co-doped ZnO by Thermal Annealing
299x254mm (72 x 72 DPI)